CHEMISTRY
A EUROPEAN JOURNAL

COMMUNICATION

DOI: 10.1002/chem.201200414

Amphiphilic Folded Dendrimer Discs and Their Thermosensitive Self-Assembly in Water

Tamer El Malah,[a, b] Simone Rolf,[c] Steffen M. Weidner,[c] Andreas F. Thünemann,*[c] and Stefan Hecht*[a]

Self-assembly is a major construction principle in nature and takes advantage of specific non-covalent interactions between custom-designed building blocks.[1] The size as well as the shape of these building blocks is crucial for the resulting assembly structure[2] and impressive examples of superstructure formation have been reported over the years.[3] In this context, shape-persistent scaffolds, in particular large (hetero)aromatic discs[4] and macrocycles[5] have been very attractive building blocks owing to their high tendency to form cofacial aggregates, that is, π-stacks,[6] either in solution or in the bulk, for example in discotic liquid crystalline phases. While these structures are rendered rigid by strong covalent bonds giving rise to annelated or macrocyclic systems, an alternative approach to construct objects with a defined conformation and hence shape relies in the use of non-covalent bonds between neighboring repeat units. Such foldamers[7] have been heavily investigated in the context of designing three-dimensional, mostly helical structures but can also lead to flat two-dimensional structures such as tapes.[8] Introducing regular branching into these folded tapes gives rise to an extension to molecular discs and hence 2D, ideally shape-persistent, folded dendrimers.[9] This approach to construct large molecular discs constitutes a non-covalent version of the covalent annelation approach of Müllen and co-workers to nanographenes, which are accessed via planarization of 3D dendritic precursors.[10] The great advantage of the folded dendrimer structure is its possible shape change in response to chemical stimuli and the ease of tuning size and amount of peripheral substitution by varying the generation.[11] In recent years, we[12] and others[13] have successfully utilized click chemistry[14] to prepare triazole connected pyridines that adopt either helically folded or zigzag tape structures. By connecting the 2,6-bis(1,2,3-triazol-4-yl)pyridine (BTP) moieties not in a linear fashion but using them as branch points this folding motif can be utilized to construct the desired dendrimer discs. Herein, we report on the synthesis and characterization of these 2D amphiphilic shape-persistent folded dendrimers and their thermosensitive self-assembly behavior in water.[15]

To efficiently construct the target dendrimer structures, a convergent synthetic route[16] was devised (Scheme 1). In our synthesis 2,6-diethynyl-4-nitropyridine serves as the key $A'B_2$ monomer, which carries two free terminal alkyne units (B), ready to couple to azide functionalities via the click reaction, and one protected focal point functionality (A′), which can be converted into an azide group. Convergent dendron growth was achieved by repetition of a sequence of twofold click reactions to the alkyne termini using previously established protocols (see the Supporting Information)[12] followed by activation of the focal point functionality via nucleophilic aromatic substitution with sodium azide. The thus prepared first three generation dendrons carrying single azide groups at their focal points were subsequently coupled to a trifunctional core, that is, 1,3,5-tri-(ethynyl)benzene to yield the target dendrimers with molecular weights exceeding 9000 D.

All dendrons and dendrimers contain polar enantiomerically pure tetra(ethylene glycol) chains[17] to provide for sufficient solubility in water and to induce circular dichroism (CD) in the course of aggregate formation, therefore facilitating analysis of the aggregation process by CD spectroscopy. Most importantly, oligo(ethylene glycol)-derived architectures[18] commonly exhibit a lower critical solution temperature (LCST),[19] rendering our dendrimers temperature-sensitive. For comparison purposes, the respective dendrimers, terminated by free carboxylic acid groups, were prepared by complete saponification of the ester side chains. All compounds were characterized by standard analytical techniques (see the Supporting Information) and investigated with regard to their aggregation behavior as pure substances. Based on some initial molecular modeling studies using molecular mechanics (MM2), due to the significant size of the systems, we anticipated the dendrimers to adopt folded two-dimensional structures giving rise to flat disc-like shapes with increasing diameter (Scheme 1, bottom). The

[a] Dr. T. El Malah, Prof. Dr. S. Hecht
Department of Chemistry, Humboldt-Universität zu Berlin
Brook-Taylor-Strasse 2, 12489 Berlin (Germany)
Fax: (+49)30-2093-6940
E-mail: sh@chemie.hu-berlin.de

[b] Dr. T. El Malah
Present address: National Research Centre
El Buhouth St., Dokki, Cairo (Egypt)

[c] S. Rolf, Dr. S. M. Weidner, Prof. Dr. A. F. Thünemann
BAM Federal Institute for Materials Research and Testing
Unter den Eichen 87, 12205 Berlin (Germany)
E-mail: andreas.thuenemann@bam.de

Supporting information for this article is available on the WWW under http://dx.doi.org/10.1002/chem.201200414.

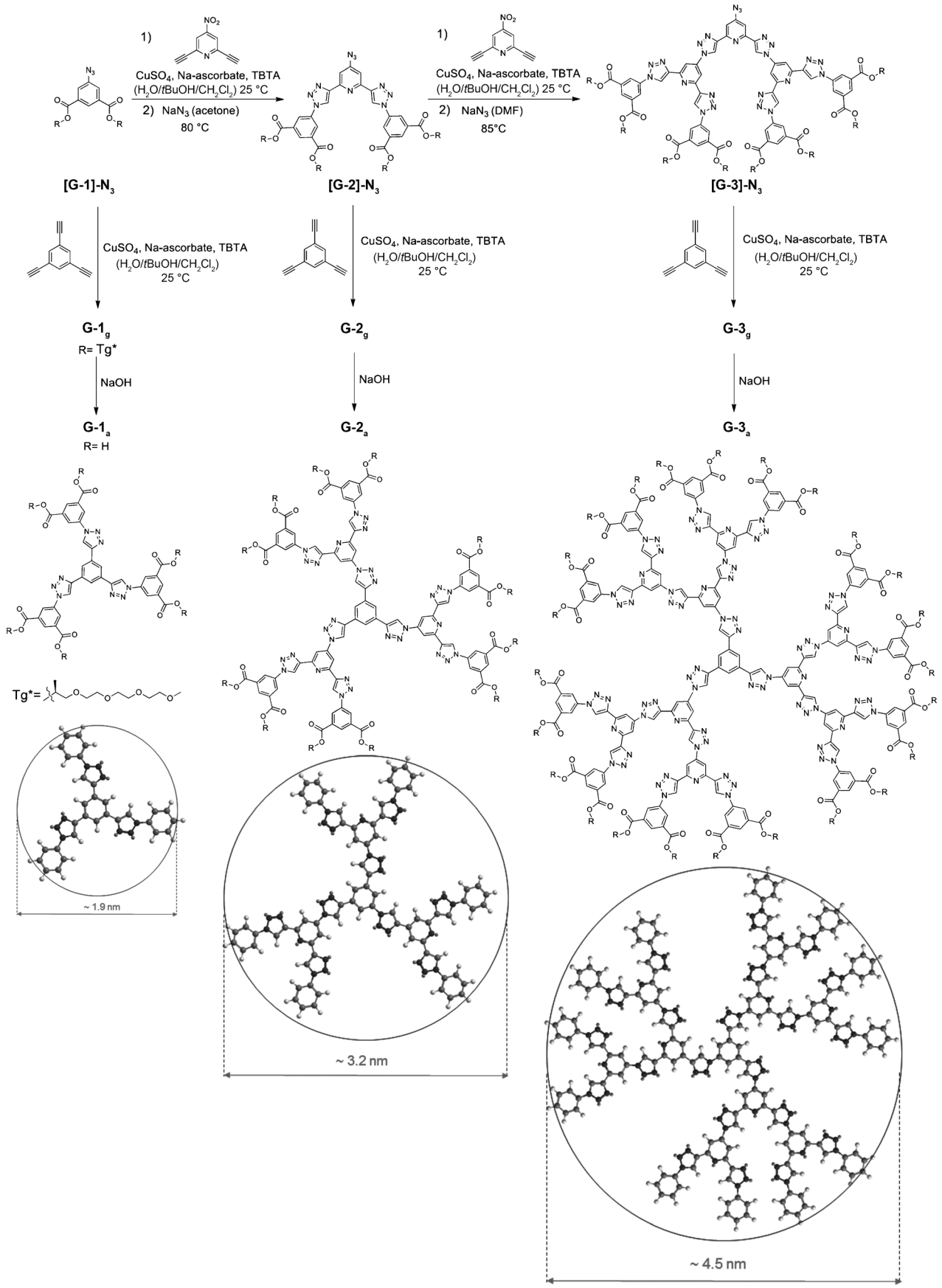

Scheme 1. Convergent synthesis of first, second, and third generation dendrons and dendrimers (**G-n$_g$** and **G-n$_a$**). Molecular models (MM2) shown were used to estimate the approximate diameters of the flat heteroaromatic dendrimer core.

dendrimers therefore resemble an amphiphilic architecture in which a rigid and extended hydrophobic heteroaromatic core with a tunable surface area is surrounded by a polar corona of flexible ether side chains. These structural features should induce self-assembly in aqueous systems and hence aggregation was studied in water to evaluate critical structural parameters (generation number) and environmental conditions (concentration, temperature).

Initially, clear aqueous solutions of the dendrimers over a broad concentration range ($8.5\cdot10^{-6}\,\text{M} \le c \le 1.6\cdot10^{-2}\,\text{M}$) became turbid upon heating above 60 °C and regained their transparency after cooling. Closer inspection of the respective absorption spectra revealed hypochromic shifts of the bands associated with the aromatic cores upon heating (see Figure S1 in the Supporting Information), thus indicating π,π-stacking. For all generations, a strong decrease of the absorbance signal was observed above 45 °C. The associated CD spectra further support these findings as strong Cotton effects, caused by chirality transfer from the side chains to the aggregate, emerge with increasing temperature. These sharp temperature-induced transitions monitored by UV/Vis and CD spectroscopy (Figure 1) are characteristic for thermosensitive polymers and show a clear dependence on the generation number and hence molecular weight.[20] Thereby, the largest dendrimer exhibits the lowest LCST, indicating the most stable aggregate in the case of **G-3$_g$**.

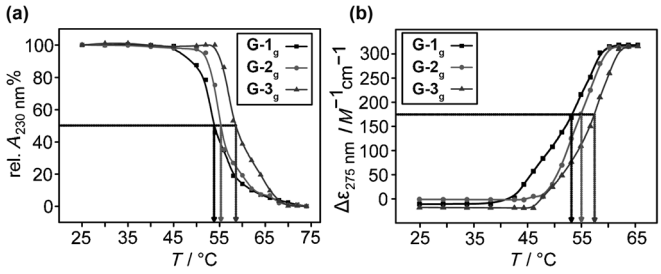

Figure 1. a) UV/Vis and b) CD spectral evolution as a function of temperature to determine the LCST for **G-n$_g$** ($c = 8.5\cdot10^{-6}$ M).

During subsequent heating-cooling cycles monitored by CD, pronounced hysteresis was observed, in particular in the case of the higher generation dendrimers (Figure 2 a). While the LCST indicates an enhanced thermodynamic stability of the aggregates for the higher generation, hysteresis suggests furthermore an increased kinetic stability, which is nicely revealed by monitoring the kinetics of disassembly (Figure 2 b). By analysis of the rates it was found that the disassembly is 34 times slower in the case of **G-3$_g$** as compared to **G-1$_g$** (see Figure S2 in the Supporting Information).

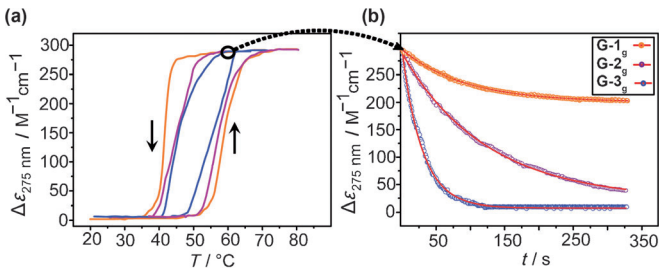

Figure 2. a) Heating–cooling cycles at 0.5 K min^{-1} and b) disassembly kinetics upon rapid cooling to 55 °C for **G-n$_g$**, as observed by CD spectroscopy ($c = 8.5\cdot10^{-6}$ M).

To gather more experimental evidence for the solution structure of the aggregates, small-angle X-ray scattering (SAXS) measurements were carried out on diluted aqueous solutions of the ester- as well as carboxylate-terminated dendrimer series **G-n$_g$** and **G-n$_a$**, respectively, at temperatures ranging from 20 °C to 80 °C. Note that the carboxylic acids **G-n$_a$** were not soluble at pH 7 and hence measured at pH 10 as their corresponding sodium salts. The scattering patterns of all dendrimers are typical for nanoparticles (Figure 3),

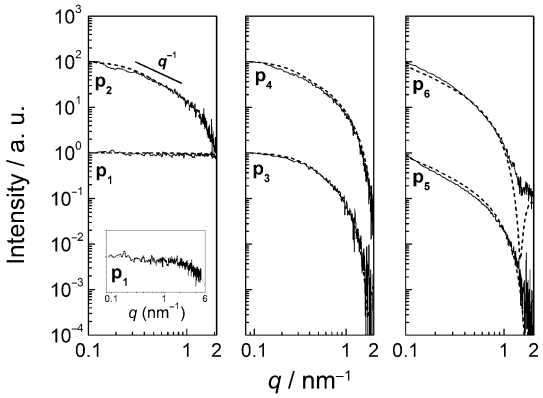

Figure 3. SAXS curves of the dendrimers (solid lines) and model curve fits (dashed lines). Upper curves are multiplied by 100 for better visibility. The inset (left bottom) shows an approximation of **G-1$_a$** (as Na^+ salt) by a homogeneous flat disk ($R = 0.35$ nm, $L = 0.15$ nm). Measurements were performed at 20 °C and concentrations were $1.6\cdot10^{-3}$ mol L^{-1} for all dendrimers (except **G-1$_a$**: $1.6\cdot10^{-2}$ mol L^{-1}).

except the one for **G-1a** being characteristic of single molecules. While the SAXS patterns of the carboxylates **G-n$_a$** are insensitive to temperature variation, the patterns of the oligo(ethylene glycol) terminated dendrimers **G-n$_g$** are constant up to a critical temperature, above which an abrupt phase separation into a water and a dendrimer phase is observed. The latter one subsequently precipitates as an insoluble white solid. This phase transition temperature is attributed to a lower critical solution temperature (LCST),[19] comparable to that observed in numerous water-soluble polymeric systems, such as poly(ethylene glycol)-based thermogels.[20] For accurate determination of the LCST transitions, temperature-dependent dynamic light scattering (DLS) experiments were carried out. The LCST transitions (Table 1) are nicely reflected by an abrupt increase of the hydrodynamic radii of **G-n$_g$** nanoparticles from ca. 10 nm to ca. 800 nm (see Figure S3 in the Supporting Information). The subsequent rapid additional increase in the sizes up to the micrometer range is accompanied by precipitation, explaining the decreasing scattering intensity.

Table 1. Structural parameters and dimensions derived from curve fits of the SAXS measurements (see Figure 3) at 20 °C, below LCST, independently measured by different techniques (DLS, UV, CD).

Dendrimer	Shape	Length [nm]	Radius [nm]	LCST [°C]		
				DLS	UV	CD
G-1$_a$	disc	ca. 0.15	ca. 0.35	–[a]	–[a]	–[a]
G-1$_g$	column	14.7 ± 0.2	1.41 ± 0.04	51	54	53
G-2$_a$	column	12.3 ± 0.5	2.20 ± 0.02	–[a]	–[a]	–[a]
G-2$_g$	column	16.8 ± 0.7	1.86 ± 0.01	52	56	55
G-3$_a$	column	58.0 ± 0.8	2.62 ± 0.01	–[a]	–[a]	–[a]
G-3$_g$	column	57.7 ± 1.0	2.31 ± 0.01	57	58	57.5

[a] No LCST Transition was detected for the carboxylate salt (pH 10).

In addition to determining the LCST transition, the SAXS data provide valuable information about the structure of the aggregates in solution. At 20 °C the form of the curves of dendrimers **G-n$_g$** are typical for a highly elongated shape of the particles where the scattering intensity in the q region from about 0.3 to 0.9 nm^{-1} scales with q^{-1} as indicated by a straight line in Figure 3. At lower q values, a Guinier region is visible, demonstrating that the total size of the nanoparticles is attainable from the data. Finally, the particle cross-section becomes visible in the high q range. The obtained SAXS curves of dendrimers **G-n$_g$** are most appropriately described by assuming a nanorod structure model. Reasonable curve fits for other simple shapes, such as spherical or disk-like nanoparticles, could not be found. By proper curve fitting(see the Supporting Information), the dimensions of the nanorods, that is, lengths and radii, could be determined (Table 1).

The radii of the nanorods increase with increasing generation number, nicely reflecting the larger size of the higher generation dendrimers. The radii of the dendrimer cores of 1.0 nm, 1.6 nm, and 2.2 nm derived from molecular modeling represent the lower limits of the radii, which upon addition of the extended chiral oligo(ethylene glycol) chains' length of ca. 0.8 nm give 1.8 nm, 2.4 nm, and 3.0 nm as upper limits for **G-1$_g$**, **G-2$_g$**, and **G-3$_g$**, respectively. Hence, the experimentally determined radii are in agreement with a structural model assuming that the cylinders are composed of stacks of flat dendrimer discs. Note that at the first glance, it is surprising that the radius of the carboxylate-terminated dendrimers is larger than their corresponding oligo(ethylene glycol)-terminated dendrimers in both the second and third generations. The relatively large radii of **G-2$_a$** and **G-3$_a$** are most likely a result of the sodium ions, which are condensed to the surface of the nanorods and therefore contribute significantly to electron density of the corona, rendering them to appear bigger while the solvated ether side chains are partially "invisible" due to their electron density matching their surroundings.[21] This interpretation is supported by the fact that the differences of the radii, that is, r(**G-2$_a$**)−r(**G-2$_g$**) = 0.34 nm and r(**G-3$_a$**)−r(**G-3$_g$**) = 0.31 nm, are the same within experimental error.

The lengths of the nanorods reflect the aggregation number, that is, how many dendrimer discs are stacked in one cylindrical column. Based on the assumption that the nanorods are composed of flat dendrimer discs (see above) spaced by a typical π,π-stacking distance of 3.5 Å,[22] the observed lengths correlate with increasing aggregation numbers for higher generation dendrimers, that is, 42, 48, and 165 for **G-1$_g$**, **G-2$_g$**, and **G-3$_g$**, respectively. While the aggregation numbers of the lower two generations are typical for poly(ethylene oxide) based surfactants,[3,15,23,24] the third generation dendrimer forms rather large aggregates. The significant increase in the aggregation number, when going from the second to the third generation, is reflected in a much higher aspect ratio, that is, length: radius ratio, for **G-3$_a$** (22) and **G-3$_g$** (25). Assuming a simple isodesmic model for aggregate growth,[3d,6] the association constant rises from K = $1.4 \cdot 10^5$ M^{-1} (for **G-2$_g$**) to K = $1.7 \cdot 10^7$ M^{-1} (for **G-3$_g$**), approaching the values of other heteroatom-containing extended π-systems, such as perylene bisimides, in water.[6,25] This strongly enhanced aggregation constant can be correlated to the significant increase of the dendrimer core's hydrophobic surface area from about 2 × 800 Å^2 (for **G-2**) to about 2 × 1520 Å^2 (for **G-3**).[6]

To test our proposed structural model, a model-free data evaluation procedure for the calculation of the radial density profile developed by Glatter,[26] was used. In a first step, we determined the cross-sectional pair distributions functions with the established indirect Fourier transformation.[27,28] The radial electron density profiles of the cylindrical micelles $\rho(r)$ were calculated in a second step using the convolution square root method implemented in DECON.[29–31] The resulting continuous density profiles, as measured from the center of the cylinders (Figure 4), show

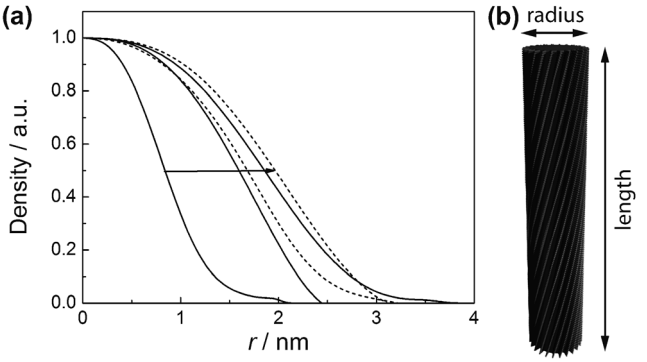

Figure 4. a) Cross-section density profiles of the nanorod as calculated with DECON.[33] The arrow traverses the curves in the order of **G-1$_g$**→**G-2$_g$**→**G-2$_a$**→**G-3$_g$**→**G-3$_a$** (solid lines indicate oligo(ethylene glycol) chain functionalized dendrimers, dashed lines indicate carboxylate-functionalized dendrimers). b) Structural model of **G-3$_g$** dendrimer aggregates with dimensions as given in Table 1.

a clear decrease of electron density towards the periphery.[32] The shift of the inflection points towards larger distances at higher generations is in agreement with the increasing radius of the dendrimer discs. Note that again the carboxylate-terminated dendrimers **G-n$_a$** appear to be more extended than the oligo(ethylene glycol) terminated dendrimers **G-n$_g$** due to the higher electron density of the sodium ions

located at the periphery.[21] On a more quantitative basis, the integrated electron density (98% for **G-1$_g$**, 97% for **G-2$_a$**, 95% for **G-2$_g$**, 98% for **G-3$_a$**, and 94% for **G-3$_g$**) is given within the radii determined by the above used simple model function. While Glatter's model-free data evaluation provides additional information on the cross-sectional structure, it nicely confirms the radii derived from applying the simple cylinder model.

Above the LCST, distinct reflections became visible in the SAXS curves (see Figure S3 in the Supporting Information), indicating that the aggregation process proceeds to structure formation on the next hierarchical level. Apparently, the nanorods pack into a 2D hexagonal columnar lattice, col$_h$, with increasing lattice constants at higher generations, that is, 3.36 nm (**G-1$_g$**), 5.10 nm (**G-2$_g$**), and 5.66 nm (**G-3$_g$**). If we further assume a dense packing of the nanorods, their radii are given by $R_c = a/2$, that is, 1.68 nm **G-1$_g$**), 2.55 nm (**G-2$_g$**), and 2.83 nm (**G-3$_g$**). When comparing these values with the radii of the nanorods found below LCST (see Table 1), we find that the radii of the nanorods in the solid state are larger than in solution. This apparent increase of the radii is most likely a consequence of the dehydrated chiral oligo (ethylene glycol) chains, which provide stronger scattering contrast in the solid as compared to their hydrated state in solution. This leads to the observed slight underestimation of the radii when using a homogeneous core nanorod model for the solution structure. The coherently scattering domain sizes of the col$_h$ phase are 311 nm (**G-1$_g$**), 15 nm (**G-2$_g$**), and 13 nm (**G-3$_g$**), as derived from the width of the (1.0) peak. The comparatively large value of the domain sizes of the first generation dendrimer is probably due to a rapid parallel alignment of its thin nanorods during precipitation. However, detailed investigations will be necessary to correlate precipitation conditions and col$_h$ ordering in the bulk and on surfaces.

Our work shows how shape-persistent flat dendrimers can be realized using non-covalent interactions in poly(triazole-pyridine) dendrimers prepared via click chemistry. Functionalization of the dendrimer periphery provides access to disc-like amphiphiles, which assemble into cylindrical stacks in water and furthermore undergo a thermosensitive phase transition from a nanorod to a col$_h$ phase. Modulation of the hydrophobic surface area of the dendrimer discs by growing different generations allows for fine-tuning of the dimensions of the nanorods and resulting aspect ratio as well as adjustment of the associated phase transition temperatures. With increasing generation number and hence association strength, the dissociation kinetics are slowed down significantly, thereby leading to a pronounced hysteresis of the CD signal, that is, chiral memory effect. Studies to elucidate the role of chirality in the assembly process are currently in progress. The demonstrated control over col$_h$ structure formation should provide new opportunities for creating well-defined and highly ordered self-assembled water-borne nanostructures. Incorporating additional function in combination with their inherent chirality renders these assemblies potentially useful templates for aqueous processes, for example the organization of inorganic semiconductors or catalysts and modification of their surfaces.

Acknowledgements

T.E.M. acknowledges the Egyptian Government for providing a doctoral fellowship. BASF AG, Bayer Industry Services, and Sasol Germany are thanked for generous donations of chemicals.

Keywords: click chemistry · Cotton effect · dendrimers · hierarchical self-assembly · thermochemistry

[1] Special issue on "Supramolecular Chemistry and Self-Assembly", *Science*, **2002**, *295*, 2400–2421 and references therein.

[2] J. N. Israelachvili, *Intermolecular and Surface Forces*, 3rd ed., Elsevier, Amsterdam, **2011**.

[3] a) L. Brunsveld, B. J. B. Folmer, E. W. Meijer, R. P. Sijbesma, *Chem. Rev.* **2001**, *101*, 4071–4097; b) F. J. M. Hoeben, P. Jonkheijm, E. W. Meijer, A. P. H. J. Schenning, *Chem. Rev.* **2005**, *105*, 1491–1546; c) J.-H. Ryu, D.-J. Hong, M. Lee, *Chem. Commun.* **2008**, 1043–1054; d) T. F. A. De Greef, M. M. J. Smulders, M. Wolffs, A. P. H. J. Schenning, R. P. Sijbesma, E. W. Meijer, *Chem. Rev.* **2009**, *109*, 5687–5754; e) B. M. Rosen, C. J. Wilson, D. A. Wilson, M. Peterca, M. R. Imam, V. Percec, *Chem. Rev.* **2009**, *109*, 6275–6540; f) C. Park, J. Lee, C. Kim, *Chem. Commun.* **2011**, *47*, 12042–12056.

[4] M. D. Watson, A. Fechtenkötter, K. Müllen, *Chem. Rev.* **2001**, *101*, 1267–1300.

[5] a) J. S. Moore, *Acc. Chem. Res.* **1997**, *30*, 402–413; b) S. Höger, *J. Polym. Sci. Part A: Polym. Chem.* **1999**, *37*, 2685–2698; c) M. M. Haley, *Top. Curr. Chem.* **1999**, *201*, 81–130; d) D. Zhao, J. S. Moore, *Chem. Commun.* **2003**, 807–818.

[6] Z. Chen, A. Lohr, C. R. Saha-Möller, F. Würthner, *Chem. Soc. Rev.* **2009**, *38*, 564–584.

[7] a) S. H. Gellman, *Acc. Chem. Res.* **1998**, *31*, 173–180; b) D. J. Hill, M. J. Mio, R. B. Prince, T. S. Hughes, J. S. Moore, *Chem. Rev.* **2001**, *101*, 3893–4011; c) *Foldamers: Structure, Properties, and Applications* (Eds.: S. Hecht, I. Huc), Wiley-VCH, Weinheim, **2007**; d) E. Yashima, K. Maeda, H. Iida, Y. Furusho, K. Nagai, *Chem. Rev.* **2009**, *109*, 6102–6211.

[8] a) M. Barboiu, J.-M. Lehn, *Proc. Natl. Acad. Sci. USA* **2002**, *99*, 5201–5206; b) Z.-T. Li, J.-L. Hou, C. Li, H.-P. Yi, *Chem. Asian J.* **2006**, *1*, 766–778; c) D. Zornik, R. M. Meudtner, T. El Malah, C. M. Thiele, S. Hecht, *Chem. Eur. J.* **2011**, *17*, 1473–1484; d) dimerization induced tape formation is highlighted by: C. Schmuck, T. Rehm in ref. 7c.

[9] a) B. Huang, J. R. Parquette, *Org. Lett.* **2000**, *2*, 239–242; b) J. Recker, D. J. Tomcik, J. R. Parquette, *J. Am. Chem. Soc.* **2000**, *122*, 10298–10307; B. Huang, M. A. Prantil, T. L. Gustafson, J. R. Parquette, *J. Am. Chem. Soc.* **2003**, *125*, 14518–14530; c) C. J. Gabriel, M. P. DeMatteo, N. M. Paul, T. Takaya, T. L. Gustafson, C. M. Hadad, J. R. Parquette, *J. Org. Chem.* **2006**, *71*, 9035–9044.

[10] For selected reviews, see: a) A. J. Berresheim, M. Müller, K. Müllen, *Chem. Rev.* **1999**, *99*, 1747–1785; b) J. Wu, W. Pisula, K. Müllen, *Chem. Rev.* **2007**, *107*, 718–747.

[11] a) G. R. Newkome, C. N. Moorefield, F. Vögtle, *Dendrimers and Dendrons. Concepts, Syntheses, Applications*, Wiley-VCH, Weinheim, **2001**; b) J. M. J. Fréchet, D. A. Tomalia, *Dendrimers and other Dendritic Polymers*, John Wiley & Sons, Chicester, **2001**.

[12] a) R. M. Meudtner, M. Ostermeier, R. Goddard, C. Limberg, S. Hecht, *Chem. Eur. J.* **2007**, *13*, 9834–9840; b) R. M. Meudtner, S. Hecht, *Angew. Chem.* **2008**, *120*, 5004–5008; *Angew. Chem. Int. Ed.* **2008**, *47*, 4926–4930; c) R. M. Meudtner, S. Hecht, *Macromol. Rapid Commun.* **2008**, *29*, 347–351; d) L. Piot, R M. Meudtner, T. El Malah, S. Hecht, P. Samorì, *Chem. Eur. J.* **2009**, *15*, 4788–4792;

e) M. Ostermeier, M.-A. Berlin, R. Meudtner, S. Demeshko, F. Meyer, C. Limberg and S. Hecht, *Chem. Eur. J.* **2010**, *16*, 10202–10213; f) ref. 8c; g) A. Cadeddu, A. Ciesielski, T. El Malah, S. Hecht, P. Samorì, *Chem. Commun.* **2011**, *47*, 10578–10580; h) T. El Malah, A. Ciesielski, L. Piot, S. I. Troyanov, U. Mueller, S. Weidner, P. Samorì, S. Hecht, *Nanoscale* **2012**, *4*, 467–472.

[13] Triazole-connected pyridine macrocycles: a) Y. Li, J. C. Huffman, A. H. Flood, *Chem. Commun.* **2007**, 2692–2694; b) Y. Li, M. Pink, J. A. Karty, A. H. Flood, *J. Am. Chem. Soc.* **2008**, *130*, 17293–17295.

[14] a) V. V. Rostovtsev, L. G. Green, V. V. Fokin, K. B. Sharpless, *Angew. Chem.* **2002**, *114*, 2708–2711; *Angew. Chem. Int. Ed.* **2002**, *41*, 2596–2599; b) C. W. Tornøe, C. Christensen, M. Meldal, *J. Org. Chem.* **2002**, *67*, 3057–2064; c) For a recent comprehensive review: M. Meldal, C. W. Tornøe, *Chem. Rev.* **2008**, *108*, 2952–3015.

[15] While self-assembly of large disc-like objects is typically studied in organic solvents, some selected examples involving π-systems appended by oligo(ethylene glycol) side chains to facilitate aggregation in water, have been reported: a) L. Brunsveld, H. Zhang, M. Glasbeek, J. A. J. M. Vekemans, E. W. Meijer, *J. Am. Chem. Soc.* **2000**, *122*, 6175–6182; b) E. Obert, M. Bellot, L. Bouteiller, F. Andrioletti, C. Lehen-Ferrenbach, F. Boue, *J. Am. Chem. Soc.* **2007**, *129*, 15601–15606; c) D.-J. Hong, E. Lee, M. Lee, *Chem. Commun.* **2007**, 1801–1803; d) K.-S. Moon, H.-J. Kim, E. Lee, M. Lee, *Angew. Chem.* **2007**, *119*, 6931–6934; *Angew. Chem. Int. Ed.* **2007**, *46*, 6807–6810; e) J.-K. Kim, E. Lee, Y.-b. Lim, M. Lee, *Angew. Chem.* **2008**, *120*, 4740–4744; *Angew. Chem. Int. Ed.* **2008**, *47*, 4662–4666. See also refs 3c,d.

[16] Original work a) C. J. Hawker, J. M. J. Frèchet, *J. Am. Chem. Soc.* **1992**, *114*, 8405–8413; b) for a review, see: S. M. Grayson, J. M. J. Frèchet, *Chem. Rev.* **2001**, *101*, 3819–3867.

[17] A. Khan, C. Kaiser, S. Hecht, *Angew. Chem.* **2006**, *118*, 1912–1915; *Angew. Chem. Int. Ed.* **2006**, *45*, 1878–1881.

[18] Selected examples of poly(ethylene glycol) terminated dendrimers: a) C. Kojima, Y. Haba, T. Fukui, K. Kono, T. Takagishi, *Macromolecules* **2003**, *36*, 2183–2186; b) C. Kojima, K. Kono, K. Maruyama, T. Takagishi, *Bioconjugate Chem.* **2000**, *11*, 910–917.

[19] N. Badi, J.-F. Lutz, *J. Controlled Release* **2009**, *140*, 224–229.

[20] For a related example, see: a) J.-F. Lutz, Ö. Akdemir, A. Hoth, *J. Am. Chem. Soc.* **2006**, *128*, 13046–13047; b) J.-F. Lutz, A. Hoth, *Macromolecules* **2006**, *39*, 893–896.

[21] A. Jusufi, M. Ballauf, *Macromol. Theory Simul.* **2006**, *15*, 193–197.

[22] Based on a typical value for π,π-stacking distances. For reviews, see: a) C. A. Hunter, K. R. Lawson, J. Perkins, C. J. Urch, *J. Chem. Soc. Perkin Trans. 2* **2001**, 651–669; b) E. A. Meyer, R. K. Castellano, F. Diederich, *Angew. Chem.* **2003**, *115*, 1244–1287; *Angew. Chem. Int. Ed.* **2003**, *42*, 1210–1250.

[23] S. V. Aathimanikandan, E. N. Savariar, S. Thayumanavan, *J. Am. Chem. Soc.* **2005**, *127*, 14922–14929.

[24] D. Orthaber, A. Bergmann, O. Glatter, *J. Appl. Crystallogr.* **2000**, *33*, 218–225.

[25] Z. Chen, PhD thesis, Universität Würzburg.

[26] O. Glatter, O. Kratky, *Small Angle X-ray Scattering*; Academic Press, London, **1982**.

[27] O. Glatter, *J. Appl. Crystallogr.* **1977**, *10*, 415–421.

[28] O. Glatter, *J. Appl. Crystallogr.* **1979**, *12*, 166–175.

[29] O. Glatter, *J. Appl. Crystallogr.* **1981**, *14*, 101–108.

[30] O. Glatter, B. Hainisch, *J. Appl. Crystallogr.* **1984**, *17*, 435–441.

[31] O. Glatter, *J. Appl. Crystallogr.* **1988**, *21*, 886–890.

[32] M. Ballauff, C. N. Likos, *Angew. Chem.* **2004**, *116*, 3060–3082; *Angew. Chem. Int. Ed.* **2004**, *43*, 2998–3020.

[33] R. Mittelbach, O. Glatter, *J. Appl. Crystallogr.* **1998**, *31*, 600–608.

Received: February 8, 2012
Published online: March 29, 2012

